PERGAMON

Chemical Engineering Science 56 (2001) 4107–4120

Chemical Engineering Science

www.elsevier.com/locate/ces

High precision prepolymerization of propylene at extremely low reaction rates—kinetics and morphology

Jochem T. M. Pater[a], Günter Weickert[a,*], Joachim Loos[b], Wim P. M. van Swaaij[a]

[a] *Faculty of Chemical Engineering, Process Technology Institute Twente/Dutch Polymer Institute, University of Twente, P.O. Box 217, NL-7500AE Enschede, The Netherlands*

[b] *Department of Chemical Engineering/Dutch Polymer Institute, Eindhoven University of Technology, P.O. Box 513, NL-5600MB Eindhoven, The Netherlands*

Abstract

A one-liter slurry phase polymerization reactor was set-up to carry out catalytic polymerizations of propylene at low reaction rates. The catalyst system used in this work was a fourth generation Ziegler–Natta catalyst, with tri-ethyl aluminum as cocatalyst and di-cyclopentyl dimethoxy silane as external electron donor. The low reaction rates allowed us to systematically study the formed particles. Polymer powder was produced with a yield of prepolymerization (YPP) varying from 0.3 g of polypropylene (PP) per gram catalyst to 50 g PP per gram catalyst. Because of the well-defined polymerization conditions, the intra- and inter-particle morphologies can be studied in order to investigate the fragmentation of the catalyst. Cross-sectional SEM pictures show a decreasing size of fragments with increasing YPP. The fragmentation does not proceed as sometimes described in literature in layers, starting from the outer layer and advancing to the center of the particle, rather the fragments are initially well distributed throughout the particle. At higher values for YPP—above 2–4 g PP per gram the size of the fragments continues to decrease with increasing YPP, but the fragments 'drift' to the outer portions of the particles. In addition to the morphological aspects, a precise study of the 'early-stage'-polymerization kinetics was carried out using measurements of monomer pressure as a function of time. Up to a YPP of about 2–4 g PP per gram catalyst, the reaction rate decreases strongly with increasing YPP, but above this value, reaction rate remains constant with increasing YPP. This effect is ascribed to a phase transition in the growing particle. Initially, the catalyst forms the continuous phase, within which the polymer is distributed. After the phase transition, the polymer forms the continuous phase in which catalyst fragments are distributed. This change causes a change in monomer concentration at the active sites, resulting in lower reaction rates. © 2001 Published by Elsevier Science Ltd.

Keywords: Kinetics; Morphology; Phase change; Polymerization; Polypropylene; Slurry phase

1. Introduction

Over the past 40 years the market for polyolefins, polyethylene and polypropylene in particular, have grown tremendously. It is also projected that this market will continue to grow as the product properties of the different materials are broadening rapidly due to new developments in both the field of catalysis and the production processes, while production costs remain relatively low.

Still, despite high expectations for large-scale introduction of metallocene catalysts, the vast majority of polypropylene is made using conventional Ziegler–Natta catalysts. These traditional catalysts currently account for about 98% of all polypropylene produced worldwide. When using titanium based catalysts supported on magnesium chloride, a prepolymerization step is often used. Prepolymerization is essentially a polymerization step performed under mild conditions and at low reaction rates. The low reaction rates allow the particle to fully activate, helps to prevent thermal runaway, and provides a controlled fragmentation of the catalyst resulting in improved particle morphology. As the major high impact polypropylene processes often make use of different polymerization reactors in series, a good particle morphology—meaning a spherical shape, a controlled porosity and a narrow particle size distribution—is

* Corresponding author. Tel.: +31-53-489-3042; fax: +31-53-489-4738.

E-mail address: g.weickert@ct.utwente.nl (G. Weickert).

0009-2509/01/$ - see front matter
PII: S0009-2509(01)00081-1

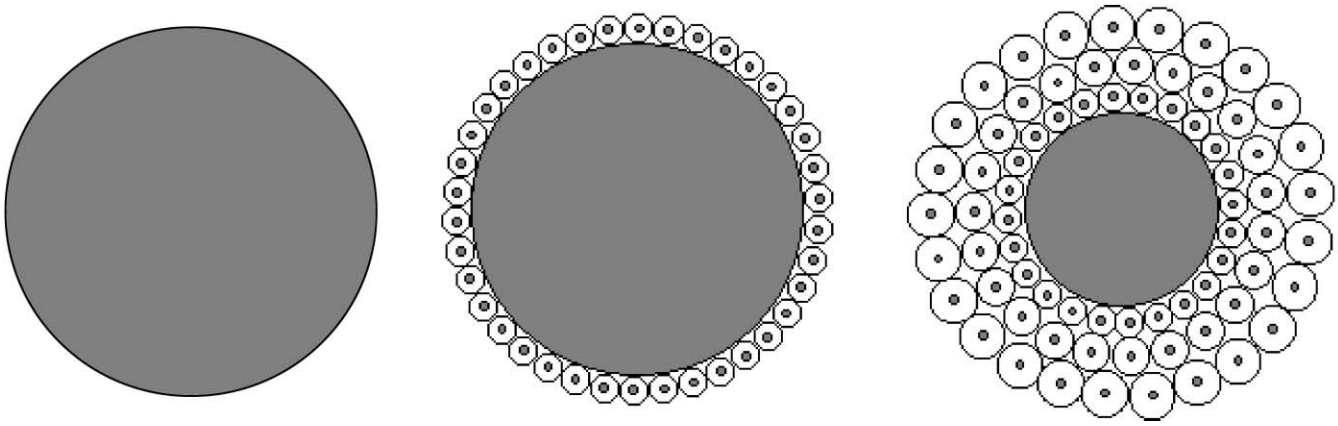

Fig. 1. Schematic representation of the fragmentation model as proposed by Ferrero and Chiovetta (1987–1991); Ferrero et al. (1992). The catalyst fragments layer wise, starting at the surface towards the core of the particle.

essential for the performance of the gas phase copolymerization reactors and distribution of the rubbery part over the homopolymer matrix. Control of particle morphology, and tools to influence this particle structure are very important. It is believed that the fragmentation of the catalyst is a decisive step in the determination of the final particle morphology, and that it can be used to control particle structure.

Due to the extreme sensitivity of modern catalyst systems to impurities and to the intrinsically high activities characteristic of olefin polymerizations, reliable and reproducible experimental results are hard to obtain in bench- or pilot-scale setups. Nevertheless, we must be able to produce the catalyst/polymer samples in a strictly controlled manner, to understand the underlying causal processes in fragmentation behavior and to study the influence of the relevant variables.

Ferrero and Chiovetta, 1987a, b; Ferrero and Chiovetta, 1991a, b; Ferrero, Koffi, Sommer, & Conner (1992) performed a series of simulations in order to understand the importance of the fragmentation stage. They proposed a model for fragmentation that assumes that the process proceeds layer by layer, starting at the surface of the particle and continuing towards the core of the catalyst macroparticle. This is illustrated in Fig. 1. In this representation, the reaction starts at the outer surface of the particle, and the polymerization front "walks" through the particle since it is assumed that polymer is produced only in the fragmented layers. This behavior leads to the conclusion that the influence of fragmentation on heat and mass transport processes is significant.

Of course, when doing experimental work on this problem, one has to keep in mind that the type of the catalyst, and specifically the nature of the support material is of utmost importance in the fragmentation behavior of the catalyst. Papers published in the area of nascent morphology of polymer particles and catalyst fragmentation clearly show the importance of the nature of the catalyst support material (Kakugo, Sadatoshi, Yokoyama, & Kojima, 1989a; Kakugo, Sadatoshi, Sakai, & Yokoyama, 1989b; Noristi, Marchetti, Baruzzi, & Sgarzi, 1994; Conner, Webb, Spanne, & Jones, 1990). It is demonstrated for example (Ferrero, Koffi, Sommer, & Conner, 1992) that a silica supported chromium catalyst shows a complete different fragmentation behavior compared to a magnesium chloride supported catalyst, most likely due to the different internal coherent forces in the support material. Apart from the nature of the support, one can imagine that the reaction rate of the polymerization can also influence the fragmentation behavior. When fractured by a blow of a hammer or within a bench-vice, a pebble will show a complete different fragmentation behavior (Weickert, Meier, Pater, & Westerterp, 1999). Such differences will occur in the various supported catalyst particles. The speed of polymer formation inside the pores of the support, and the corresponding internal stress built-up rate will change the way the catalyst fragments. In most previous studies on the development of the particle morphology reaction rates are not mentioned at all. Usually, a polymer sample is characterized by the original properties of the catalyst and the polymer yield per unit of catalyst weight only.

In the present work we show a method that allows measurements of reaction kinetics in the earliest stage of the polymerization very accurately. The experiments are stopped at well-defined yields—or yield of prepolymerization (YPP), expressed in grams of polymer per gram catalyst (support included)—and the polymer samples are analyzed and characterized. The reaction rates used here are extremely low, thereby enabling us to see the fragmentation behavior of the catalyst particles at low rates.

2. Experimental

2.1. Chemicals

The catalyst used in this work is a commercially available fourth generation, see Moore (1996), Ziegler–Natta

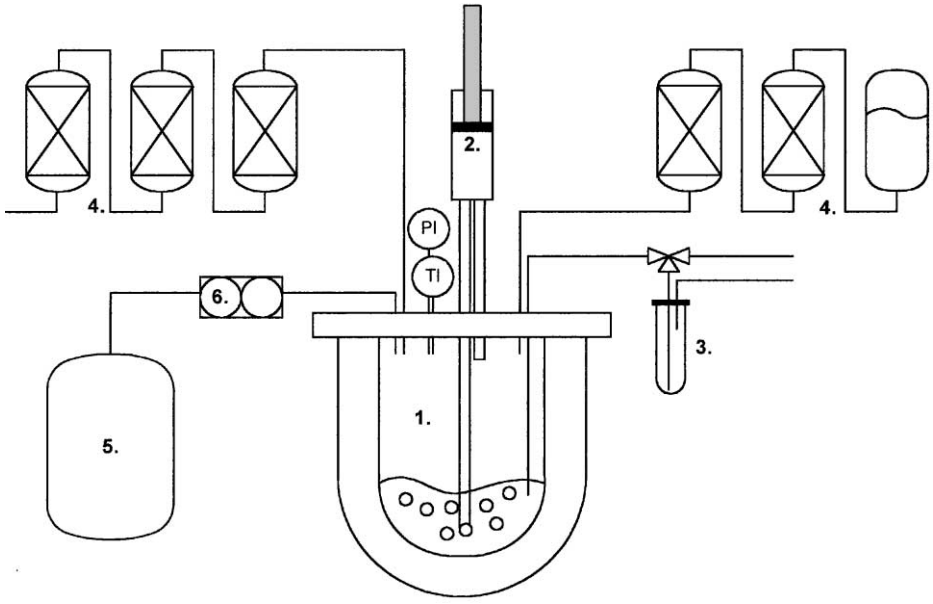

Fig. 2. Experimental set-up represented schematically used in this work. 1. Slurry phase bubble reactor, 2. Gas recirculation membrane pump, 3. Catalyst introduction system, 4. Gas and hexane purification columns, 5. Monomer vessel, 6. Mass flow controller for monomer injection.

catalyst on an $MgCl_2$ support. Tri-ethyl aluminum (kindly donated by Witco GmbH) was used as the co-catalyst, and di-cyclo pentyl di-methoxy silane (the so-called D-donor) was used as the electron donor. The catalyst components are prepared in a glove box under nitrogen. 'Pro Analysi' quality hexane (Merck) was used to suspend the catalyst. Propylene was obtained from Indugas with a purity $> 99.5\%$, with propane as main impurity. The hydrogen and nitrogen used were of $> 99.999\%$ purity.

The hydrogen, nitrogen and hexane were extra purified by passing them over a reduced BTS copper catalyst and subsequent passing through three different beds of molecular sieves, with pore sizes of 13, 4 and 3 Å, respectively. The BTS catalyst was obtained from BASF. The propylene was purified in the same way, after which it was passed through a bed of oxidized BTS copper catalyst to remove carbon monoxide.

2.2. Experimental set-up

A scheme of the experimental setup used in this work is represented in Fig. 2. The polymerization experiments were carried out in the 1-l glass reactor (1). One hundred and fifty ml of hexane were used in the experiments to suspend the catalyst–polymer particles. A membrane gas circulation pump (2) was used to stir the slurry. This provides effective mixing, but with much lower local shear stresses that would be observed with a standard magnetic bar stirrer. The injection system (3) allows the components of the catalyst system to be introduced into the reactor without exposing them to the atmosphere. Reaction gases are all purified again before use in the experiment by molecular sieves and copper catalysts (4). The polymerization is started by injecting pulses of monomer from the monomer reservoir (5), through the mass flow controller (6) to the reactor.

2.3. Polymerization

The glass reactor is heated overnight at 120°C. Then, just before performing a polymerization, it is connected to the rest of the experimental system, and cleaned by subjecting it to a vacuum for 5 min and flushing it with nitrogen at a temperature of 90°C. After cleaning, the reactor is tested for gas leakage and filled with hexane.

The different components of the catalyst system are prepared in the glovebox under nitrogen. The catalyst, suspended in a mineral oil, is weighed in a vial and diluted with hexane. The aluminum alkyl and the D-donor are weighed in separate vials, and both diluted with hexane. After the reactor has been filled with 100 ml of hexane, the alkyl and the donor are introduced. The components are contacted in the reactor for 20 min at room temperature. At the end of the contact time, the catalyst is introduced. The liquid volume after introduction of the catalyst is 150 ml. Once the catalyst has been contacted for 15 min with the diluted co-catalyst and electron donor, the monomer is injected and the polymerization reaction starts.

Injection of a pulse of monomer leads to an increase of the reactor pressure. Once the pressure comes to equilibrium, pressure measurements can be used to monitor the reaction rate, as described below. Reactor temperature and pressure data are saved to the hard disk of the

data acquisition unit every 5 s, together with jacket inlet and outlet temperatures.

After an experiment, that is typically comprised of 3 or more monomer injections, the resulting polymer powder is removed from the slurry reactor and reintroduced into the glovebox. The material is then washed several times with fresh hexane to remove aluminum alkyl and donor, deactivated by introduction of small amounts of air to the suspension and subsequently dried by slow evaporation of the hexane.

2.4. Determination of reaction rate in slurry phase

Monitoring of pressure and temperatures begins directly after the catalyst has been added to the system. Before injection of the monomer, the total pressure in the reactor consists of two contributions: the vapor pressure of the hexane and the inert nitrogen present in the system. With information on temperature these two terms can be determined, using the well-known law of Raoult:

$$P_{\mathrm{Hex}} = x_{\mathrm{Hex}} P^0_{\mathrm{Hex}}, \tag{1}$$

where P^0_{Hex} is the partial pressure of pure hexane at the specific temperature T and P_{Hex} the actual partial pressure of hexane at mole fraction x_{Hex}. When a pulse of monomer is added to the reactor, the pressure increases. After equilibrium is reached, the total reactor pressure consists of three contributions: vapor pressure of hexane and partial pressures of nitrogen and propylene. The vapor pressure of the propylene is calculated using Henry's law, as the propylene is only present at very low mole fractions:

$$P_{\mathrm{PPY}} = x_{\mathrm{PPY}} H \tag{2}$$

with P_{PPY} being the partial pressure of the propylene at mole fraction x_{PPY}, and H as the Henry's Law coefficient. Therefore, the total reactor pressure P_R can be defined with Eqs. (3) and (4), before and after monomer addition, respectively. The moment of monomer injection is said to be $t = 0$.

$$t = 0 \qquad P_R = P_{N_2} + P^0_{\mathrm{Hex}}, \tag{3}$$

$$t > 0 \qquad P_R = P_{N_2} + (1 - x_{\mathrm{PPY}}) P^0_{\mathrm{Hex}} + x_{\mathrm{PPY}} H. \tag{4}$$

With information on the solubility of propylene in hexane, these three terms can be determined fairly accurately, and therefore the amount of unreacted propylene is known at every moment in time. The reaction rate is thus defined

$$R_p(t) = \frac{[m_{\mathrm{PPY}}(t) - m_{\mathrm{PPY}}(t + \Delta t)]}{m^*_{\mathrm{catalyst}} \Delta t}, \tag{5}$$

with m_{PPY} and m_{catalyst} being the mass of unreacted propylene present in the system and the mass of the catalyst, respectively. Because of the fact that this differential method is sensitive to small variations in the pressure registration, results can be improved by smoothing the measured pressure curve, using a fitting tool. Fig. 3 shows both the raw pressure curve and the smoothed version. It can be seen that when the noise disappears, results from calculations will gain accuracy, even at small pressure differences below 0.1 bar.

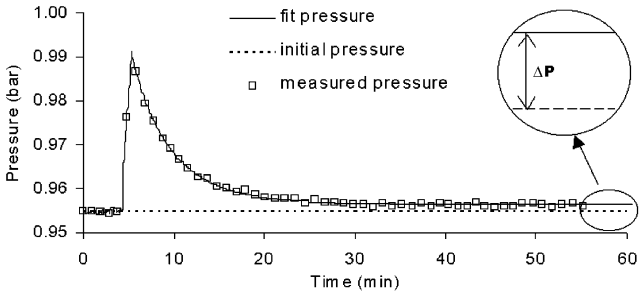

Fig. 3. Typical pressure curve versus time for a dose of monomer, with measured data, smoothed pressure curve and initial pressure level.

2.5. Cross-sectional SEM

The morphologies of the samples were investigated using a Philips environmental scanning electron microscope XL-30 ESEM FEG (Phillips, Eindhoven, The Netherlands) equipped with energy dispersive X-ray spectrometer (EDX) for local and area distribution analyses of elements. Secondary electron (SE) imaging of the samples surfaces was performed in high vacuum mode using acceleration voltages of 1 kV, whereas qualitative EDX analysis were carried out in wet mode at accelerating voltages of 5, 10 and 20 kV, respectively. For both cases, no additional coating of the sample surface was done because charging is not an issue for the chosen imaging conditions. For an acceleration voltage of 1 kV, the penetration of the incident electron beam is in the order of a few tens of nanometers for the materials in question, therefore, in addition to standard high acceleration voltage scanning electron microscopy, SE images acquired at 1 kV acceleration voltage show surface features in more details, even at high magnification, whereas wet mode renders EDX analysis without coating of non-conductive samples unnecessary.

Samples were embedded in epoxy resin and cut at room temperature, to obtain cross-sectional pictures of the polymer particles.

3. Results and discussion

3.1. Equilibrium propylene and hexane

It is assumed that the gas and liquid phases are in equilibrium during the polymerization. Equilibrium data of the hexane–nitrogen–propylene system are needed in

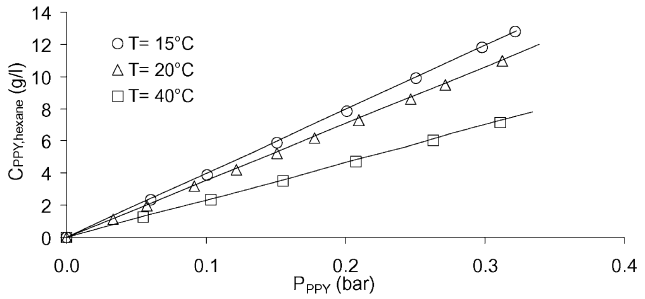

Fig. 4. Solubility of propylene in hexane at various temperatures. The markers were obtained from measurements, the lines resulted from HYSYS-calculations, with the Peng-Robinson EOS.

order to calculate the amount of propylene present in the reactor from the reactor pressure. Measurements were performed without catalyst components using Eqs. (1), (3) and (4). Fig. 4 shows that the equilibrium can be well described by Henry's law. HYSYS calculations, also shown in this figure, show excellent agreement with these measurements. The Henry's-law coefficient describing the equilibrium was determined at different temperatures, and it was shown that the temperature dependence of this coefficient can be modeled linearly over the narrow range of temperatures of interest in this work:

$$H = 0.221T - 55.32. \quad (6)$$

This relation was then used to translate data on reactor pressure to amounts of monomer by using Eqs. (1)–(4).

3.2. Pre-polymerization kinetics

As mentioned before, the kinetic data presented here are the result of different monomer injections within the same experiments. In the initial stage after monomer injection, the pressure decrease is used to calculate the reaction rate in that stage of the experiment. As pressure becomes extremely small in the final stage of the pulse, calculations are no longer reliable.

Although a total of approximately 40 experiments were performed in this study, we will only present the results of the 14 most illustrative runs here for reasons of clarity. Nevertheless, it should be pointed out here that the results presented below are representative of all the experiments. The recipes and experimental conditions used in these tests are shown in Table 1. It can be seen from this table that the amount of monomer used per injection, and the amount of catalyst used in each experiment vary over a relatively wide range. This was done in order to obtain a large variation in the final values of YPP and reaction times. However, the Al/Ti and Al/Si ratios were kept constant at 12 and 3.4 mol/mol, respectively in all experiments.

3.3. Typical pressure curve

A typical curve is shown in Fig. 3 for the reactor pressure over time. It can be seen that the pressure rises with monomer injection, and then drops due to consumption of the monomer. On the right hand side of this same figure, it can be seen that the final pressure does not return to the initial pressure before injection. This is due to two factors:

- Formation of the polymer. The solid polymer material will occupy reactor volume and will cause a pressure increase with increasing yield. This will give an increase in pressure of about 30 Pa per injection.
- Injection of inert gases with monomer. The injected propylene contains about 0.5% propane and some various amount of solved nitrogen due to transport of the liquid propylene with nitrogen at elevated pressures. This will cause a momentary increase of reactor pressure with monomer injection. This will give an increase in pressure of about 25 Pa per injection.

Corrections in the pressure measurements were made for these two factors, and are taken into account in the kinetic data presented here. The polymer volume will increase with YPP and with time, and the pressure increase due to inert gases occurs directly after each monomer injection.

3.3.1. Reproducibility

The reproducibility of the polymerization kinetics was examined by performing three experiments with the same procedure and recipe (experiments 1, 2 and 3 in Table 1). Fig. 5 shows the kinetic results calculated from these experiments. The reaction rate, corrected for the monomer concentration in the bulk was plotted versus YPP. It can be seen that the results are highly reproducible, despite the extremely low reaction rates. The reaction rate decreases with increasing YPP, and appears to be of first order with respect to monomer concentration. A calculated standard deviation of the data from the first monomer pulse gives 0.76. The maximum deviation in Fig. 5 is 6%. The reason for plotting the reaction rate versus the YPP values instead of plotting it versus time is described below.

3.3.2. Relation reaction rate and time

Fig. 6 shows the development of the reaction rate corrected for the monomer concentration related to reaction time. It is clear that the reaction rate decreases strongly in the course of an experiment. There can be a number of different causes for this behavior, of which chemical deactivation of the active sites, caused for example by over-reduction of titanium sites by the aluminum alkyl, is one. If a chemical process were causing the decreasing reaction rate one would expect a clear relation between this deactivation and reaction time. In literature, a simplified model is often used to describe the kinetics of these

Table 1
Overview of experiments presented in this work

Exp. (—)	Temperature (°C)	Duration (min)	Catalyst (mg)	Al/Ti (mol/mol)	Al/Si (mol/mol)	# pulses (-)	PPY (mg)	YPP (g/g)
1	20	140	151.1	11.9	3.4	4	921	6.10
2	20	120	150.3	11.9	3.3	3	691	4.60
3	20	140	151.4	11.7	3.4	4	921	6.08
4	20	180	150.1	11.8	3.2	6	1500	9.99
5	20	130	600.3	11.8	3.4	2	192	0.32
6	20	130	300.4	11.8	3.4	2	219	0.73
7	20	100	88.0	10.4	3.3	3	397	4.51
8	20	165	151.5	11.9	3.3	8	1050	6.93
9	20	75	150.2	11.8	3.3	1	301	2.00
10	20	150	152.0	11.6	3.2	3	744	4.89
11	20	150	150.1	11.8	3.3	4	1701	11.33
12	20	240	150.0	11.8	3.4	5	3136	20.91
13	20	75	151.0	11.9	3.4	1	454	3.01
14	20	120	150.8	11.8	3.4	8	935	6.20

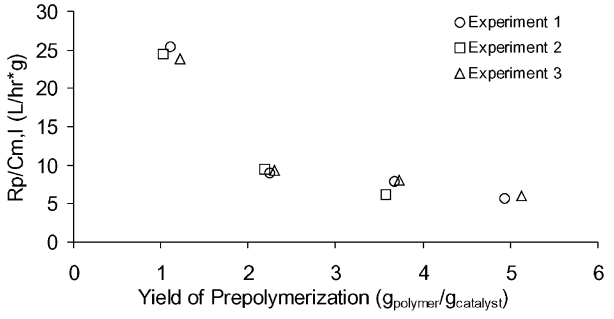

Fig. 5. An indication for the reproducibility of the kinetic results. The three experiments were exactly the same in method and recipe.

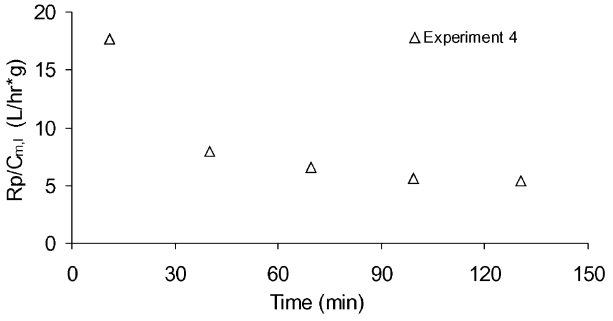

Fig. 6. Typical time dependence of the reaction rate corrected for the monomer concentration.

polymerization reactions, e.g., Meier (2000) or Samson, Weickert, Heerze, and Westerterp (1998). In the model used in these two papers, the propagation rates of the different active sites are lumped into a single propagation parameter and the different deactivation mechanisms are lumped into a single deactivation parameter. The reaction rate is represented as

$$R_p = k_p C_m^n C^* \quad \text{or} \quad \frac{R_p}{C^*} = k_p C_m^n \qquad \text{(7a and b)}$$

with an Arrhenius temperature dependence of the propagation constant:

$$k_p = k_{p,0} e^{(E_{a,p}/RT)}, \qquad (8)$$

where k_p is the propagation rate constant, $E_{a,p}$ is the activation energy for the lumped propagation reactions, T is the temperature, C_m represents the concentration of the monomer at the active site and C^* is the concentration of the active centers. In many studies, the reaction rate has been confirmed to follow a first-order dependence with respect to the monomer concentration, so n being one. The decay of the catalyst is described by a decreasing number of active centers with time, according to the following mathematical equation that has only an empirical meaning:

$$-\frac{dC^*}{dt} = k_d (C^*)^q \qquad (9)$$

with an Arrhenius type of temperature dependence of the deactivation constant k_d:

$$k_d = k_{d,0} e^{(E_{a,d}/RT)}, \qquad (10)$$

where q is the order of deactivation, $E_{a,d}$ is the activation energy for the lumped deactivation reactions. Combination of Eqs. (7) and (9) leads to:

$$-\frac{dC^*}{dt} = k_d \left(\frac{R_p}{k_p C_m^n}\right)^q. \qquad (11)$$

After integration assuming isothermal conditions and first order deactivation ($q = 1$), the expression for the reaction rate as function of time is given by

$$R_p = R_{p,0} e^{-k_d t} \qquad (12)$$

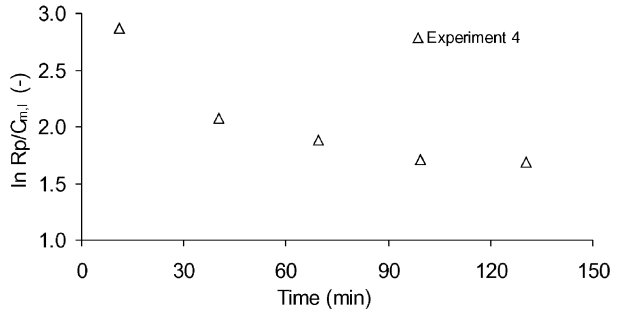

Fig. 7. Assuming a first order deactivation behavior in time, the relation between the natural logarithm of reaction rate and time should be linear, which it is not.

with

$$R_{p,0} = k_{p,0} e^{-E_{a,d}/RT} C_0^* C_m \quad (13)$$

with C_0^* being the initial concentration of active sites.

In the experiments shown here, the monomer concentration is not constant over time. When assuming a first order dependence of reaction rate in monomer concentration (i.e., $n = 1$) the kinetics—being the product of k_p and C^*—can be evaluated by using R_p/C_m in the kinetic plots, as shown in Eq. (7b).

If the deactivation of the catalyst observed in these experiments could be described with the model presented above, a linear relation should exist between the natural logarithm of the reaction rate corrected for the monomer concentration and time. However, it is shown in Fig. 7 that no such linearity exists. The decrease of corrected reaction rate with time is relatively strong in the initial stage, but levels off and finally becomes zero. A time defined process, such as a chemical reaction does not seem to be the main reason for the decreasing reaction rate.

In this work, a number of experiments were carried out using different quantities of catalyst amounts and varying sizes of the monomer pulses to the system. Fig. 8 shows a graph of the corrected rates versus experimental time for 3 such experiments. It can be seen here that the decay in reaction rate does not depend on time. A factor of at least 5 exists between reaction rates observed at catalyst amount of 90 mg, compared to a catalyst amount of 300 mg, despite the fact that the reaction rate is expressed per amount of catalyst.

3.3.3. Relation reaction rate and yield of prepolymerization (YPP)

If the same experiments are plotted in relation to the YPP as done in Fig. 9, we can see that the three experiments show exactly the same behavior. Recall that the experiments shown in this figure have very different reaction time—YPP behaviors. Fig. 10 shows the increase of the YPP values versus time for the different experiments. Despite these differences, the experiments show a similar

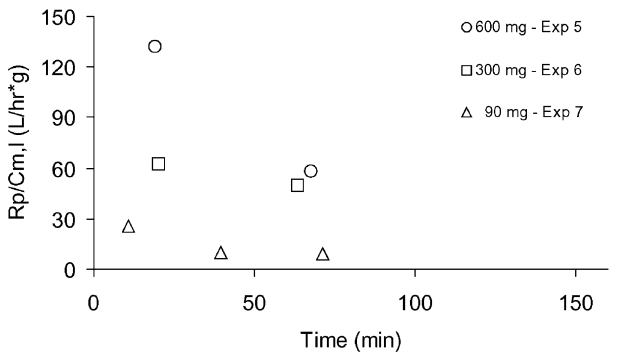

Fig. 8. Reaction rate corrected for monomer concentration versus time for three different amounts of catalyst used. In comparing these experiments, a factor of 5 can be seen in the differences in reaction rates.

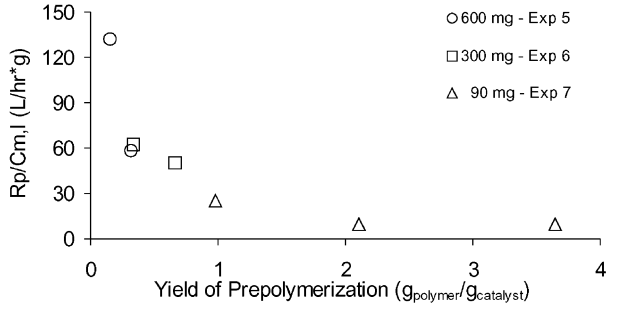

Fig. 9. Reaction rate corrected for monomer concentration versus the yield of prepolymerization for three different amounts of catalyst.

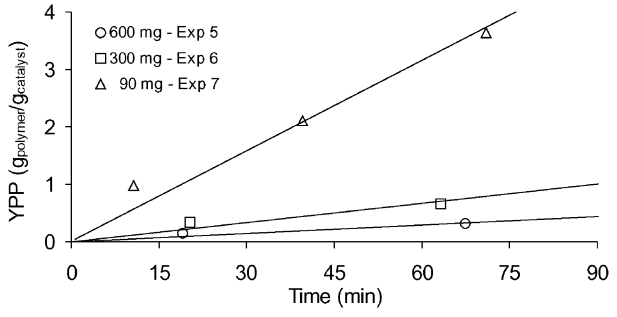

Fig. 10. Relation between yield of prepolymerization and time for the different experiments. The overall reaction rate for an experiment, including a number of monomer injections—so the slope of the lines—was varied over a wide range in these experiments.

deactivation behaviors, suggesting that the decay in reaction rate depends on the amount of polymer produced in the catalyst particle, not on the reaction time.

Complicating the explanation of the experimental observations is the fact that when plotting the monomer-corrected reaction rates of a single injection versus time, a constant slope is obtained. Despite the fact that the YPP value is increasing, the reaction rate does

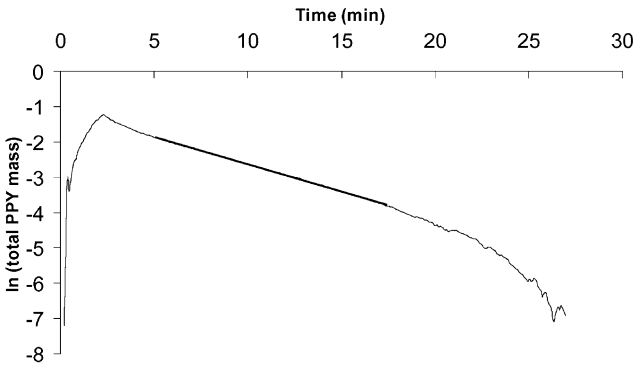

Fig. 11. The natural logarithm of the amount of monomer plotted versus time. The linear behavior up to more than 90% conversion does not agree with the decreasing reaction rates with increasing YPP values.

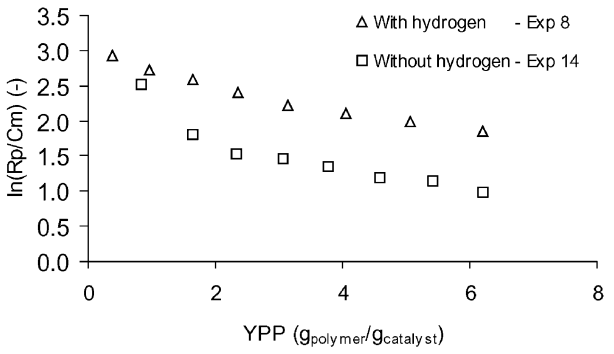

Fig. 12. Influence of hydrogen on activity and deactivation in the polymerization experiment. It can be seen that the decay in reaction rate is not changed by the introduction of the hydrogen.

not decrease during this single peak, but rather decreases over the course of different peaks. This effect can be illustrated when the integral method for kinetic evaluation is used, instead of the differential method. The natural logarithm of the amount of propylene present in the system is plotted versus time in Fig. 11. It can be seen that after stopping the injection and coming to equilibrium, a linear relation is obtained. At very low reaction rates (i.e., where more than 90% of the monomer initially present has then been consumed), the linearity disappears. In the linear stage, the reaction rate does not decrease with increasing YPP. A possible explanation for this would be the presence of fast reacting impurities in the propylene, resulting in reduced activity after every injection. But as the reaction rate becomes constant at higher YPP values, and no longer decreases upon injection of fresh monomer, this cannot be the case.

Two different mechanisms were proposed to explain the decreasing reaction rate with increasing YPP. It is generally accepted that the catalyst as used here is sensitive to 2,1-insertions of propylene, resulting in a dormant state of the active sites. As the initial propagation frequency in these experiments is in the order of 0.1–10 monomer molecules per second, one could imagine that the decay of catalyst activity with increasing yield in the early stage of the polymerization reaction, could be the result of an increasing number of active sites blocked by 2,1-inserted monomer. In the initial stage of the experiment, the number of dormant sites increases with increasing YPP, but at higher YPP values, all the sites that are sensitive to 2,1-insertions are dormant and the activity of the overall catalyst reaches a constant level. If this mechanism is the reason for the strong catalyst decay in the initial stage, the phenomenon should disappear, or should at least be significantly diminished, in the presence of a chain transfer agent like hydrogen. The hypothesis was tested in an experiment in the presence of hydrogen. In this experiment, the hydrogen concentration was about 10 vol% in gas phase, and thus well within the range where hydrogen concentration normally does not affect the reaction rate. The result of this run, experiment 14, is shown in Fig. 12. It is clear that the activity in the presence of hydrogen is significantly higher than in the absence of the hydrogen, but both curves seem to show the same initial reaction rate. With hydrogen present, the decay seems to be less strong and therefore come to a higher final value. It is therefore possible that the number of dormant sites increases with increasing YPP in the absence of hydrogen, and that this effect is prevented in experiment 14. However, even in presence of hydrogen the effect of the decreasing activity with increasing YPP, especially for YPP values below 2–4 g/g is similar. Therefore, another explanation for these observations must be found.

Another explanation for the decrease in reaction rate in the early stage of the polymerization, is the ‘phase transition’ that the growing particle undergoes during this period. Initially, the particles are made up essentially of support material, and only a small amount of polymer is present in the matrix. With increasing YPP, the particle is gradually transformed from a “support-dominated” material to a polymer particle with small amounts of catalyst. This significant change in morphology and the change of the kinetics seem to occur at the same time. To the best of our knowledge, no description of this behavior appears in the literature on catalytic olefin polymerization. This ‘phase transition’ could influence different factors in the polymerization process.

- The active site of the catalyst is formed by an interaction between the external electron donor, the co-catalyst and the catalyst itself. One could easily imagine that large amounts of polymer produced at this site could very well change this interaction, and with that the kinetic behavior of the site. This diluting effect caused by the polymer could play a role in the decreasing reaction rates.
- Another factor that is changing with the ‘phase transition’ is the monomer concentration at the active

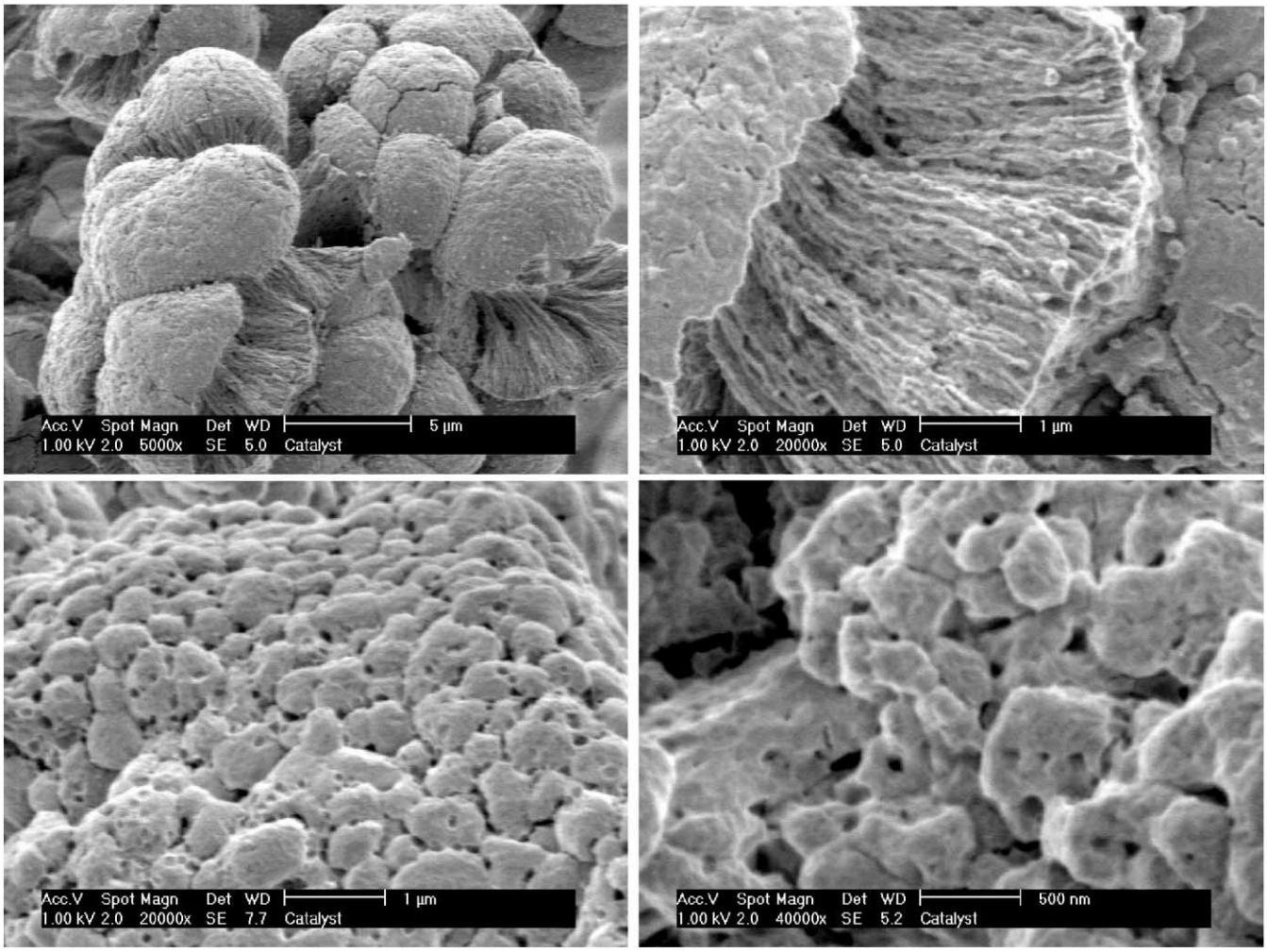

Fig. 13. These SEM pictures show the structure of the catalyst material used in the experiments.

site. If we assume that a fresh, initially active site is surrounded by hexane with a bulk monomer concentration, the concentration at the active site equals this bulk concentration. With progressing polymerization, the number of active sites surrounded by polymer increases. For the active sites surrounded by polymer, it holds that the concentration of monomer at the active site equals the monomer concentration sorbed in the polymeric phase. So, with an increasing YPP, the number of active sites seeing a low monomer concentration increases and results in a decreasing reaction rate.

If the changes in morphology and in kinetics come together in the initial stage of polymerization, this effect should be present in all polymerization reactions with this type of catalysts. But as reaction rates are normally some orders of magnitude larger than the reaction rate used here and almost all methods used to measure reaction rates are unreliable in the unstable initial stage of the experiment, this effect cannot be observed there.

3.4. Morphology of polymer particles

The powders produced in the experiments presented above were analyzed with electron microscopy. SEM micrographs were made of the outer surface of the particles to show the developing shape of the particles, and to see the particle sizes. In addition, some particles were embedded in an epoxy resin and cut to allow imaging of the cross-sectional surface of the polymer particles.

Fig. 13 shows the SEM pictures of the catalyst material. The structure of the catalyst support can be well seen. The material is very porous and the radial pores with diameters around 0.1 micron are clearly visible. The catalyst particles appear to be made up of 15–30 smaller spheres. The catalyst particles are around 25 microns in diameter, with the diameter of the smaller spheres on the order of 5–10 micron.

Fig. 14 shows the particles after polymerization. The particle sizes obviously increase due to the accumulation

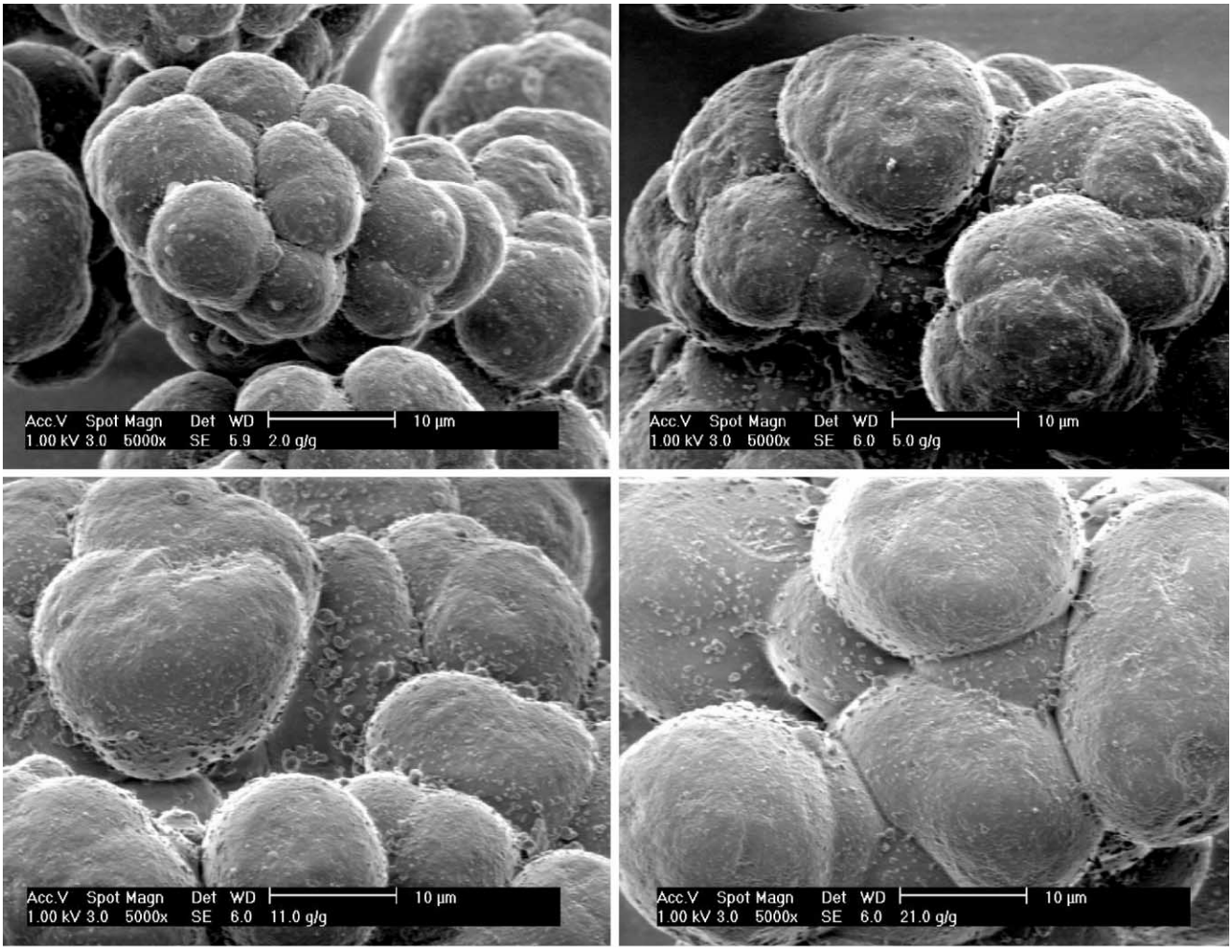

Fig. 14. SEM pictures of prepolymerized catalyst particles, with respectively a yield of prepolymerization of 2, 5, 11 and 21 g/g.

of polymer. The four pictures in Fig. 14 show particles with YPP values of 2, 5, 11 and 21 g polymer per gram catalyst. There is a high degree of replication, as the shape of the polymer particles is almost identical to the shape of the initial catalyst particles. The smaller spheres from which the particle is made up can clearly be recognized. The size of the particles systematically increases with increasing YPP, as shown in Table 2.

The SEM images in Fig. 15 show the cross sectional surface of the polymer particle after cutting; the sphere shown on the picture of the cross sectional cut is one of the spheres of which the particle is composed. Two phases can be recognized in the cut surfaces. The gray, continuous phase is assumed to be polymer material, the drop-like heterogeneous phase with the lighter color is believed to be support material. There are several arguments for this explanation. The ratio between the amount of homogeneous and heterogeneous phase is, within the possible accuracy of such 2-dimensional surface determination, in accordance with the values for YPP. Preliminary EDX tests also showed a high concentration of magnesium in the light colored areas and, when electron microscopy was performed in the presence of an

Table 2
Development of theoretical particle size of the sub-particle with increasing YPP

YPP (g_{PP}/g_{cat})	Radius (micron)	$Volume_{particle}$ ($micron^3$)	$Volume_{catalyst}$ ($micron^3$)	$Volume_{polymer}$ ($micron^3$)
0	5.0	524	524	0
1	7.6	1873	524	1350
2	9.2	3223	524	2699
3	10.3	4573	524	4049
5	12.0	7272	524	6748
7	13.4	9971	524	9448
10	15.0	14020	524	13497
15	17.1	20769	524	20245
20	18.7	27517	524	26994
30	21.4	41014	524	40490
40	23.5	54511	524	53987
50	25.3	68008	524	67484

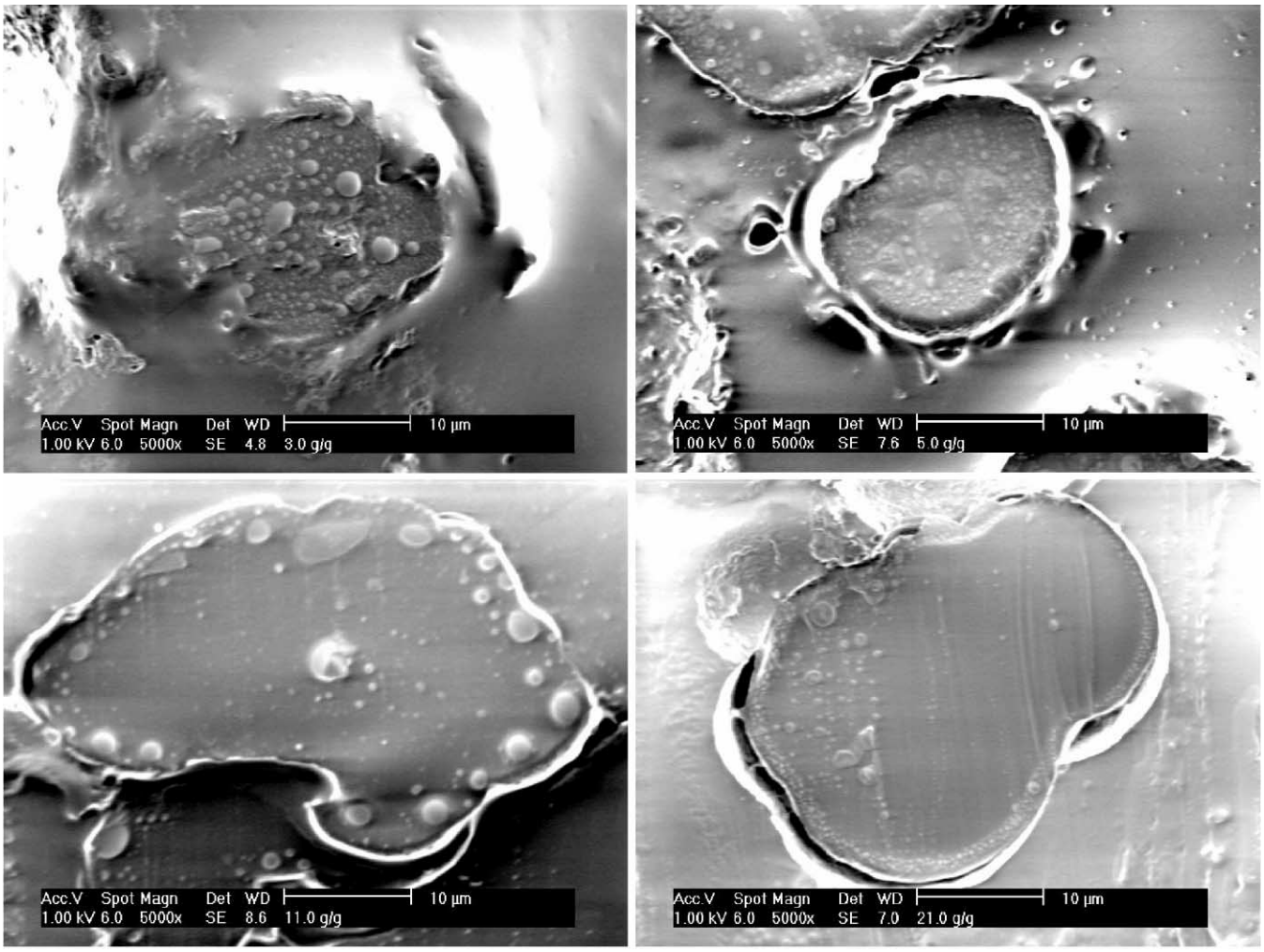

Fig. 15. Cross sectional SEM pictures of prepolymerized catalyst particles with yield of prepolymerization of respectively 3, 5, 11 and 21 g/g.

oxygen-containing atmosphere, these areas changed color rapidly and a salty structure appeared in the light colored areas.

It can also be seen that the support fragments decrease in size with increasing YPP values. It seems as if fragmentation of the catalyst is continually progressing in the stage we visualized here. One thing that is remarkable is the place where the fragments are located in the growing particles. The fragments seem to tend to drift to the outside of the particles. In contrast to fragmentation models described in literature by Ferrero and Chiovetta (1987–1991), Ferrero et al. (1992) the fragmentation of the support used here does not proceed shell-by-shell from the outside of the particle towards the center. Rather, the particle seems to break into large fragments first, and subsequently with progressing polymerization the fragments increase in number and decrease in size. In their later work related to this subject (Ferrero et al., 1992) an experimental study is shown with polymer powders with YPP values between 29 and 114 g/g, obtained in slurry polymerization of propylene in heptane. It is mentioned in their work that with the experimental data obtained it was not possible to confirm nor to disprove the sequential layer-by-layer type of fragmentation. We think that fragmentation model can be disproved by the data shown here, at least for the catalyst and the reaction conditions used here.

Of course, one has to keep in mind that the pictures shown here are not pictures in a continuous series. The different experiments used to reach different YPP values differ from each other in monomer concentrations and therefore in reaction rates. One can imagine that fragmentation behavior depends on reaction rate. It is therefore hard to conclude that particles in, for example, low temperature liquid pool polymerization typical of industrial prepolymerization conditions will look like the particles shown here. Reaction rates under those conditions are typically in the order of a few kilogram of polymer per gram catalyst and hour, so much higher than reaction rates used here. To be able to make an even

Table 3
Values for yield average monomer concentration in experiments with shown SEM pictures, related to YPP values obtained in those experiments

Exp.	YPP	Yield average monomer concentration (g/l)			
(—)	(g/g)	Pulse 1	Pulse 2	Pulse 3	Pulse 4
9	2.0	0.24	—	—	—
10	4.9	0.17	0.32	0.45	—
11	11.3	0.31	0.60	0.58	0.86
12	20.9	0.28	0.54	0.60	0.60
13	3.0	0.57	—	—	—

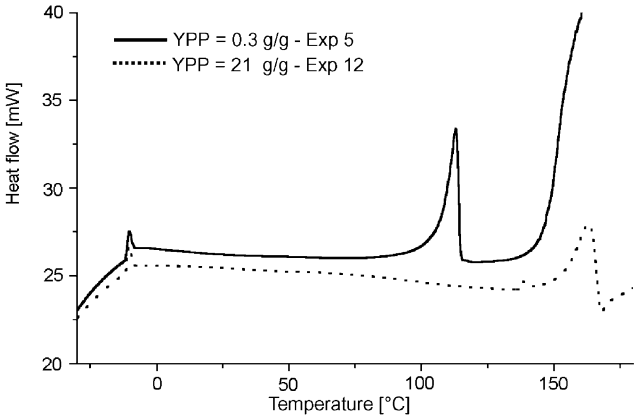

Fig. 16. DSC curves of polymer products with low and with high YPP values.

more meaningful comparison, one should use a stopped flow method in liquid pool conditions, to be able to stop the polymerization reaction after seconds, and thus to produce particles with YPP values comparable to the ones shown here.

In the pictures of the particles with low YPP values, below 3 g/g, a wax-like material can be observed on the surface of the particles. When this substance was observed, it was very difficult to cut the particles we embedded in resin for cross-sectional examination by SEM as the cut surface was always located within this wax-like layer, and not across the polymer particle. In experiments yielding in higher YPP values this problem was not present. An explanation for the formation of this poor material is given in the monomer concentration. Because of the fact that monomer concentration is not constant during the polymerization experiments and polymer properties will depend on the monomer concentration during polymerization, it is hard to quantify the monomer concentration for a specific polymer product, for a specific YPP value. Here the average monomer concentration as defined by the formula in Eq. (14) is used to characterize the monomer concentration during the experiment. An experiment with a high initial monomer concentration after a large injection of monomer also has a rate curve with a low activity tail caused by low monomer concentration. Since the amount of polymer produced at a certain monomer concentration is important in order to understand the molecular weight, we used the 'yield average monomer concentration', $C_{m,\mathrm{Yield}}$, as an indication of the "average" monomer concentration in a given experiment:

$$C_{m,\mathrm{Yield}} = \frac{\sum(\mathrm{Yield}_j C_{m,j})}{\sum \mathrm{Yield}_j}, \tag{14}$$

where Yield_j represents the amount of polymer produced in a certain interval at monomer concentration $C_{m,j}$. For the experiments shown here, the yield average monomer concentrations (YAMC) are shown in Table 3. It can be seen that in experiments designed to produce a final powder with low YPP values, the values for YAMC were much lower than the YAMC values in experiments resulting in high YPP values. These low values for YAMC are probably the main cause for the formation of the waxy product with a poor stereospecificy. Fig. 16 shows the DSC curves of the polymer products with low YPP values and that of polymer with a high YPP value. The additional peak at 115°C is expected to be caused by the atactic material, produced at the low monomer concentration in the experiments with low YPPs.

4. Conclusions

The experimental method demonstrated in this paper has shown to be a useful tool in the investigation of the processes implicated in the very early stage of catalyzed olefin polymerizations. The kinetics can be measured with a high reproducibility and, because of the good control of the polymerization rate, the reaction can be stopped at well defined, low yields. It is shown that in the very early stage of the polymerization of this type of catalyst, the reaction rates drop significantly with increasing YPP. It is expected that this behavior is related with the changing morphology in this early stage and that it is present in all polymerizations with this type of catalyst. It is difficult to observe this type of behavior and to do this type of experiment with conventional polymerization equipment because of the extremely high reaction rates observed during typical polymerization procedures. In the experiments presented here, reaction rates become stable with increasing YPP after reaching a value of about 2–4 g polymer per gram catalyst.

The SEM pictures of the cross-sectional areas of the polymerized particles suggest that the "layer- by-layer" fragmentation models proposed in literature do not ade-

quately describe fragmentation of the catalyst used in this work under our experimental conditions.

To be able to draw conclusions on fragmentation behavior at higher reaction rates, it is necessary to carry out stopped flow polymerizations in liquid propylene. The powders obtained from such experiments should be investigated the same way as done here. It is not possible to measure kinetics in the initial stage of the polymerization that way, but it should clarify the reaction rate dependency of the fragmentation mechanism.

Notation

C^*	concentration of active sites, mol/g
C_m	concentration of monomer, g/l
$C_{m,\mathrm{Yield}}$	yield average monomer concentration, g/l
$E_{a,p}$	activation energy for the lumped propagation reactions, J/mol
$E_{a,d}$	activation energy for the lumped deactivation reactions, J/mol
H	Henry's-law coefficient, bar
k_d	deactivation rate constant, h^{-1}
k_p	propagation rate constant, l/mol h
m	mass, g
n	order of propagation, —
q	order of deactivation, —
P	pressure, bar
P^0	saturated vapor pressure, bar
R	gas constant, J/mol K
R_p	reaction rate of polymerization, g/g h
T	temperature, K
t	time, h
x	mole fraction, —
Yield_j	amount of polymer produced in interval j, with $C_{m,j}$, g

Subscripts

0	initial, at time = 0
hex	related to hexane
ppy	related to propylene
catalyst	related to the catalyst
N_2	related to the nitrogen
R	reactor

Abbreviations

Al	aluminum
D-donor	di-cyclopentyl di-methoxy silane
EDX	energy dispersive X-ray
PP	polypropylene
PPY	propylene
SEM	scanning electron microscopy
Si	silane, in external electron donor
TEA	tri ethyl aluminum
Ti	titanium
YAMC	yield average monomer concentration
YPP	yield of prepolymerization

Acknowledgements

The work presented in this paper was carried out in corporation with The Dow Chemical Company, Freeport (TX), USA. The authors wish to thank Dow for both the financial and the intellectual input. The aluminum alkyls used in the work were kindly donated by Witco GmbH, Bergkamen, Germany.

This work would not have been completed without the experimental work carried out by Suzanne Huibers, Harriet Workel and Jantina de Waal. In addition, the technical assistance of Fred ter Borg, Karst van Bree and Geert Monnink of the High Pressure Laboratories is gratefully kindly acknowledged.

References

Conner, W. C., Webb, S. W., Spanne, P., & Jones, K. W. (1990). Use of X-ray microscopy and synchroton microtomography to characterize polyethylene polymerization particles. *Macromolecules*, *23*, 4742–4747.

Ferrero, M. A., & Chiovetta, M. G. (1987a). Catalyst fragmentation during propylene polymerization: Part I. The effects of grain size and structure. *Polymerization Engineering Science*, *27*, 1436–1447.

Ferrero, M. A., & Chiovetta, M. G. (1987b). Catalyst fragmentation during propylene polymerization: Part II. Microparticle diffusion and reaction effects. *Polymerization Engineering Science*, *27*, 1448–1460.

Ferrero, M. A., & Chiovetta, M. G. (1991a). Effects of catalyst fragmentation during propylene polymerization IV Comparison between gas phase and bulk polymerization processes. *Polymerization Engineering Science*, *31*, 904–911.

Ferrero, M. A., & Chiovetta, M. G. (1991b). Catalyst fragmentation during propylene polymerization III bulk polymerization process simulation. *Polymerization Engineering Science*, *31*(12), 886–903.

Ferrero, M. A., Koffi, E., Sommer, R., & Conner, W. C. (1992). Characterization of changes in the initial morphology for $MgCl_2$-supported Ziegler–Natta polymerization catalysts. *Journal of Polymer Science: Part A: Polymer Chemistry*, *30*, 2131–2141.

Kakugo, M., Sadatoshi, H., Yokoyama, M., & Kojima, K. (1989a). Transmission electron microscopic observation of nascent polypropylene particles using a new staining method. *Macromelecules*, *22*, 547–551.

Kakugo, M., Sadatoshi, H., Sakai, J., & Yokoyama, M. (1989b). Growth of polypropylene particles in heterogeneous Ziegler–Natta polymerization. *Macromolecules*, *22*, 3172–3177.

Meier, G. B. (2000). *Fluidized bed reactor for catalytic olefin polymerization*. Ph.D. thesis at University of Twente, pp. 5–35.

Noristi, L., Marchetti, E., Baruzzi, G., & Sgarzi, P. (1994). Investigation on the particle growth mechanism in propylene

polymerization with $MgCl_2$-supported Ziegler–Natta catalysts. *Journal of Polymer Science: Part A Polymer Chemistry*, *32*, 3047–3059.

Samson, J. J. C., Weickert, G., Heerze, A. E., & Westerterp, K. R. (1998). Liquid-phase polymerization of propylene with a highly active catalyst. *A.I.Ch.E. Journal*, *44*(6), 1424–1437.

Weickert, G., Meier, G. B., Pater, J. T. M., & Westerterp, K. R. (1999). The particle as microreactor: catalytic propylene polymerizations with supported metallocenes and Ziegler–Natta catalysts. *Chemical Engineering Science*, *54*, 3291–3296.